Structural Engineering and Mechanics, *Vol. 58, No. 6 (2016) 1021-1044*
DOI: http://dx.doi.org/10.12989/sem.2016.58.6.1021

Damage and fatigue quantification of RC structures

Kabir Sadeghi* and Fatemeh Nouban[a]

Civil Engineering Department, Near East University, Near East Boulevard, ZIP: 99138, Nicosia, North Cyprus, Mersin 10, Turkey

(Received February 8, 2016, Revised March 17, 2016, Accepted March 27, 2016)

Abstract. Different versions of a damage index (DI) along with a formulation to find the number of cycles at failure due to fatigue, applicable to reinforced concrete (RC) structures are presented. These are based on an energetic analysis method and applicable to both global and local levels. The required data can be found either from the numerical simulation of structures or from the experimental tests. A computer program has been developed to simulate numerically the nonlinear behavior of RC columns under cyclic loading. The proposed DI gives a regular distribution of structural damages up to failure and is validated by the results of the tests carried out on RC columns subjected to cyclic loading. In general, the local and global damage indices give approximately similar results, while each of them has its own advantages. The advantage of the implicit version of DI is that, it allows the comparison of the results with those of the monotonic loading case, while the explicit version makes it possible to estimate the number of loading cycles at failure due to fatigue, and the advantage of the simplified version is that; the monotonic loading data is not needed for the cyclic loading case.

Keywords: reinforced concrete; structures, earthquake, fatigue, damage, cyclic loading, failure

1. Introduction

Different types of structures, during their service life, accumulate damage resulting from the actions of various environmental cyclic loading and impacts. The cumulative damage causes changes in the properties of the structural system, especially in the case of an earthquake or fatigue loading.

The technical rules and practice codes accept a certain amount of damage in the structural members during seismic vibrations. The use of a DI enables the quantification of the structural damage caused by earthquakes or the other cyclic loading.

Existing damage indices are based on different characteristics such as the number of cycles (Palmgren-Miner, Shah, Oh and Chung), stiffness (Lybas, Roufaiel and Meyer), ductility (Park, Gupta, Bertero) and energy (Banon, Darwin, Park and Meyer) and do not indicate correctly the real sequence or amount of damage.

Within the energy-based damage indices, the DI proposed by Meyer (1988) is oversensitive to

*Corresponding author, Associate Professor, E-mail: kabir.sadeghi@neu.edu.tr, kabirsadeghi@gmail.com
[a]Ph.D., E-mail: fatemeh.nouban@neu.edu.tr, f.nouban@gmail.com

http://www.techno-press.org/?journal=sem&subpage=8 ISSN: 1225-4568 (Print), 1598-6217 (Online)

the number of cycles and is, therefore, not applicable in the case of loading comprising repeated cycles. The DI proposed by Park and Ang (1985) which is based on the plastic-hinge approach and consists of both deformation and energy terms, has been criticized by Abbasnia *et al*. (2011) and some other researchers.

The global DI proposed by Amziane and Dubé (2008) is applicable to RC structures under uniaxial cyclic bending with axial load. Massumi and Monavari (2013) have proposed an energy-based method to obtain the target displacement for reinforced concrete frames under cyclic loading assuming that the capacity of energy absorbing of the structures for both the pushover and cyclic analyses are equal.

In some of the existing global energy-based damage indices (proposed by Meyer 1988, Garstka 1993 and also in the implicit and explicit versions presented in this paper), monotonic loading test is needed for the cyclic loading cases because in these damage indices, absorbed energy to failure of monotonic loading is used as normalizing factor for cyclic loading cases, therefore some adaptation measures are also required. Meyer has fixed the extreme limits of DI (zero and 100% at intact and failure states), but the distribution of DI between zero and 100% especially for repeated cycles is not valid. In the implicit and explicit versions of the DI presented in this paper, a monotonic normalizing factor is used. In the implicit version, in addition to usage of a normalizing monotonic factor, an adaptation factor is also used. In the simplified version of DI, the cyclic normalizing factor is used and therefore no adaptation factor is needed. Rodrigueza and Padillaa (2009) have proposed a DI for the seismic analysis of RC members using the hysteretic energy dissipated by a structural member and a drift ratio related to the failure of the structure. The index was calibrated against observed damage in laboratory tests of RC columns under various protocols. An analysis of the parameters involved in the definition of their proposed DI showed the importance of displacement history in the drift ratio capacity of structures. Paal *et al*. (2014) presented a method of automatically determining the damage state of RC columns in RC frame buildings based only on the automatically detected damage and column information. In addition, their proposed method automatically determines the residual drift capacity. All of the methods previously developed by the writers were combined with the method newly presented by them and the results were compared with those of manual assessment procedures. Iranmanesh and Ansari (2014) reported on the development of a methodology to evaluate the energy dissipation in reinforced concrete columns with circular cross sections based on the curvatures measured in the plastic hinge area. The scope of their study included the evaluation of their proposed damage assessment method through hybrid simulation tests on hybrid models of a two-span bridge subjected to various amplitudes of near-source ground motions of the 1994 Northridge earthquake. Cao *et al*. (2014) briefly reviewed all available concepts and investigated their relative merits and limitations with a view to proposing a new concept based on residual deformation. They proposed a DI based on energy, both for static and for cyclic loadings, are compared with those obtained using the most widely accepted DI in literature. Their proposed DI demonstrated a rational way to predict the extent of damage for a number of case studies.

Fatigue damage in RC structures is mainly a problem in practical engineering, the fatigue failure mechanism rather than the destruction of the static bearing capacity mechanism is complex and influenced by many factors. A large number of experimental data shows that the fatigue life of the concrete beam is random and the use of probability and reliability theories are required to analyze it. Fatigue failure of the concrete elements is gradually accumulated within the damaged material. This cumulative process is usually an irreversible and a random energy dissipation process. Therefore, the correct description of the material subjected to cyclic loading, fatigue

damage accumulation process, and the material fatigue life estimates should be carried out. Li *et al*. (2015) have experimentally investigated the fatigue performance of RC beams with hot-rolled ribbed fine-grained steel bars under static and constant-amplitude cyclic loading. Test results indicate that, the concrete beams, reinforced with the appropriate amount of HRBF500 bars, can survive 2.5 million cycles of constant-amplitude cyclic loading with no apparent signs of damage, provided that the initial extreme tensile stress in the steel bars was controlled to less than 150 MPa. They also found that, the initial extreme tension steel stress, stress range, and steel ratio were the main factors that affected the fatigue properties of RC beams with HRBF500 bars, while the cross-sectional shape had no significant influence on fatigue properties. Zhu *et al*. (2014) have proposed a procedure for fatigue reliability prediction of PSC highway bridges. Vehicle-bridge coupling vibration analysis was performed for obtaining the equivalent moment ranges of a critical section of bridges under typical fatigue truck models. Three-dimensional nonlinear mathematical models of fatigue trucks are simplified as an eleven-degree-of-freedom system. The limit state functions are constructed according to the Miner's linear damage rule, the time-dependent S-N curves of prestressing tendons and the site-specific stress cycle prediction. Currently, the engineering community has widely used fatigue cumulative damage theory and Miner's linear cumulative damage theory proposed by Palmgren. The use of Miner theory is based on the traditional stress-life curves and stress-number (SN) curves to determine the failure of the structures (Changfeng *et al*. 2012). In Eurocode there are two alternative methods by which fatigue in reinforced concrete can be calculated: The Cumulative Damage Method, and the λ-Coefficient Method. Both methods consider the loading during the lifetime of a structure, but in a different manner. The Cumulative Damage Method calculates a fatigue damage factor which expresses the actual damage occurred in the structure in relation to the design fatigue life. The λ-Coefficient Method simply checks if the structure fulfills the demands of a given service life (Olsson and Peterson 2010, Amaravel and AppaRao 2015).

The goal of this paper is to present the different versions of a global and a local DI for RC structures subjected to monotonic, cyclic and fatigue loading. The implicit, explicit and simplified versions of an energy based DI along with a formulation of the number of cycles at failure for fatigue indices are presented in this paper. The different versions of the proposed DI are applicable for monotonic, cyclic and fatigue loading cases.

2. Experimental data

The proposed DI and the numerical simulation have mainly been validated by the experimental test results of Garcia Gonzalez performed on the full-scale columns (Garcia Gonzalez 1990, Sieffert *et al*. 1990). Over 20 tests were performed on columns under biaxial alternating cyclic with axial loading. This column is fixed at the bottom, free at the top and is under an axial force of 500 kN and a cyclic oriented lateral force and axial loading (COLFAL) or an oriented pushover force and axial loading (OPFAL) in any direction at the top. The horizontal loads through different orientations Ω have been applied on the top of the columns.

3. Developed computer program

A computer program entitled Column Analysis and Damage Evaluation Program (CADEP) has

been developed by the authors to simulate numerically the behavior of RC columns under cyclic loading and DI for rectangular or nonrectangular sections, considering the nonlinear behavior of materials.

CADEP has some sub-programs such as BBCS (biaxial bending column simulation) which is used as Base Model, CCS (confined concrete simulation), UCS (unconfined concrete simulation), SBS (steel bars simulation), EC (energy calculation) and DIC (damage index calculation).

In the proposed simulation algorithm used in the CADEP computer program, the column is decomposed into two Macro-Elements (ME) positioned between the inflection point (zero moment) and the critical sections (maxim moments). Then the nonlinear behavior of ME are analyzed. In fact, a Macro-Element acts as fixed bottom-free top half-column under biaxial cyclic bending moment (i.e., lateral force in any direction) with axial load. Finally, the two connected ME are assembled to determine the global behavior of the column. To find the status of the entire column, the applied loads and also the secondary moments, due to P-Δ effect, are considered in the simulation of the column. Each section of the column is discretized into fixed rectangular finite elements. For each concrete and reinforcement element a uniaxial behavior is considered and their strain distributions are assumed to form a plane which remains a plane during deformation (Kinematics Navier's hypothesis). The stresses of concrete and steel are expressed as nonlinear functions of strains in each concrete and steel element. For compressive confined and unconfined concrete elements, the cyclic stress-strain model proposed by Sadeghi (2014) and for reinforcements, the expression proposed by Park and Kent (1972) based on the Ramberg-Osgood cyclic model have been used in the proposed simulation algorithm. The concrete tensile stress is assumed to be linear up to the concrete tensile strength. The CEB Code (1978) specification is used for the maximum compressive strain value for unconfined concrete. This is particularly applicable where there is a loss of concrete cover outside the stirrups. To determine the failure of confined concrete in the simulation, the equation proposed by Sheikh (1982) has been used.

The basic equilibrium is justified over a critical hypothetical cross-section assuming the Navier law with an average curvature. The method used qualifies as a "strain plane control process" that requires the resolution of a quasi-static simultaneous equations system using a triple iteration process over the strains (Sadeghi 2015). The calculations are based on the cyclic nonlinear stress-strain relationships for concrete and reinforcement FE. In order to reach equilibrium, three main strain parameters; the strains at the extreme compressive point, the strains at the extreme tensile point and the strain at a point located at another corner of the section are used as three main variables. For non-rectangular sections these points may be outside the actual cross-sections and be located on the discretizing mesh frontiers.

The nonlinear responses of a Macro-Element and the column are based mainly on the fixed finite elements at the critical sections and on the location of the inflection point. For the entire column, deflection is evaluated using an elastic-plastic analytic formulation (Priestley and Park 1987). The program takes into account the confining effect of the transverse reinforcement and simulates the loss of the concrete cover. The CADEP allows the determination of the failure, the internal local behavior of critical sections (i.e., strains, stresses, neutral axis position, cracks positions, loss of material, microscopic DI, etc.) and the external global behavior of the column (curvature, deflection, stiffness, damping ratio, different types of energies for negative and positive displacements, global and local damage indices, etc., Sadeghi 2015).

The simulated results obtained using CADEP are confirmed with the full-scale experimental results obtained by other researchers (Garcia Gonzalez 1990, Sieffert *et al*. 1990, Park and Kent 1972).

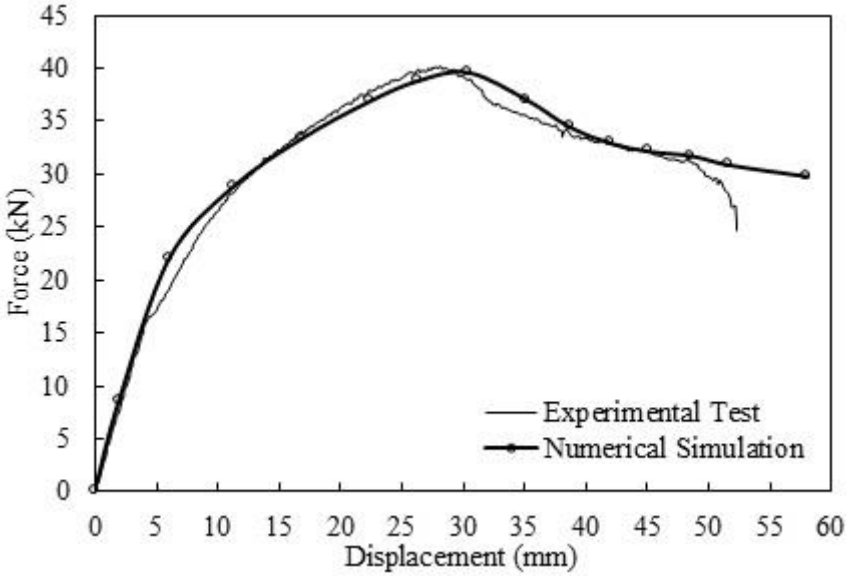

Fig. 1 Comparison of the proposed simulation and experimental test results, BMAL case

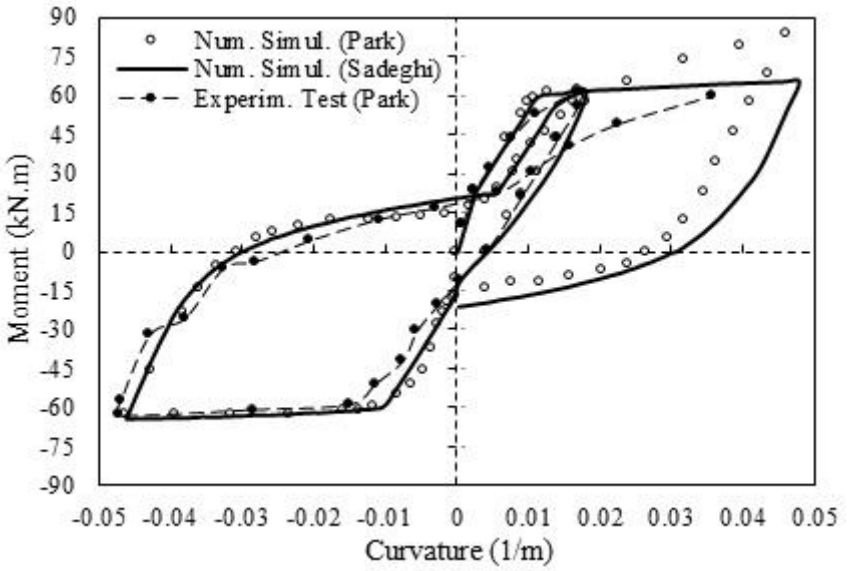

Fig. 2 Comparison of proposed simulation and experimental test/simulation of Park and Kent (1972), CBM case

Comparison of numerically simulated results using the proposed simulation algorithm and experimental tests on full-scale RC members are reflected in Figs. 1 and 2. The comparison indicates a good agreement between the proposed simulation and the experimental test results. In Fig. 1, the results of the proposed simulation are compared with the experimental test results of Garcia Gonzalez (1990), Sieffert *et al*. (1990) on the columns tested under Bending Moment and Axial Loading (BMAL). In Fig. 2, the results of the proposed simulation and experimental

test/simulation of Park and Kent (1972) for a Cyclic Bending Moment (CBM) loading case are compared. As these figures show there is a good agreement between simulated and experimental results.

4. Proposed damage index

4.1 Description of the steps

To find and evaluate the proposed DI, the various steps applied are as follows:
- studying the different types of energies to find the weighting, importance and the role of different types of energy in the damage extension and DI,
- evaluating the relationship between damages for displacements in the positive and negative directions as well as the overall damage,
- concentrating on the similarities and differences between monotonic and cyclic loading,
- studying and choosing a normalizing factor,
- the proposition of a DI,
- evaluation of the proposed DI by using the experimental tests and simulated results.

4.2 Concepts of "Primary half-cycle" and "following half-cycle" absorbed energy

The absorbed energy in each cycle of loading number "*i*" is divided into two parts: the primary half-cycle absorbed energy (E_{pi}) and the following half-cycle absorbed energy (E_{fi}). Their physical meanings are described below by introducing the concepts of "primary half-cycle" (PHC) and "following half-cycle" (FHC). After Otes (1985) a "primary half-cycle" is considered when any half-cycle reaches a new maximum amplitude; it is followed by a certain number of "following half-cycles" with smaller amplitudes. Whenever a certain maximum displacement $(\delta_{\max})_i$, corresponding to the primary half-cycle $(PHC)_i$ is exceeded, a new primary half-cycle $(PHC)_{i+1}$ is established. Every PHC corresponds to a certain damage degree. For more information about the practical application of the PHC and FHC absorbed energies please refer to the schematic example given in Section 4.5**.**

4.3 Analyzing different types of energy

In order to consider the weighting, importance and the role of different types of energy in the DI, the different energies extracted from the experimental tests and numerical simulation were analyzed and compared, as listed below:
- Absorbed energy "E_a" (area under the force-displacement curve. See also section 4.5),
- Dissipated energy "E_d" during cyclic loading (force-displacement hysteresis loop area),
- Recovered energy "E_r" (the difference between "E_a" and "E_d". See also section 4.5),
- PHC absorbed energy "E_p", (see sections 4.2 and 4.5),
- FHC absorbed energy "E_f", (see sections 4.2 and 4.5).

The variations of the above-mentioned energies versus top horizontal displacements for column C0C3 under the cyclic loading are illustrated in Fig. 3.

As shown in Fig. 3, the ratio $\sum_{i=1}^{i=i} E_{fi}^{+}/\sum_{i=1}^{i=i} E_{pi}^{+}$ is approximately equal to 185. This is one of the reasons that the FHC absorbed energy effect should be considered only implicitly (not directly)

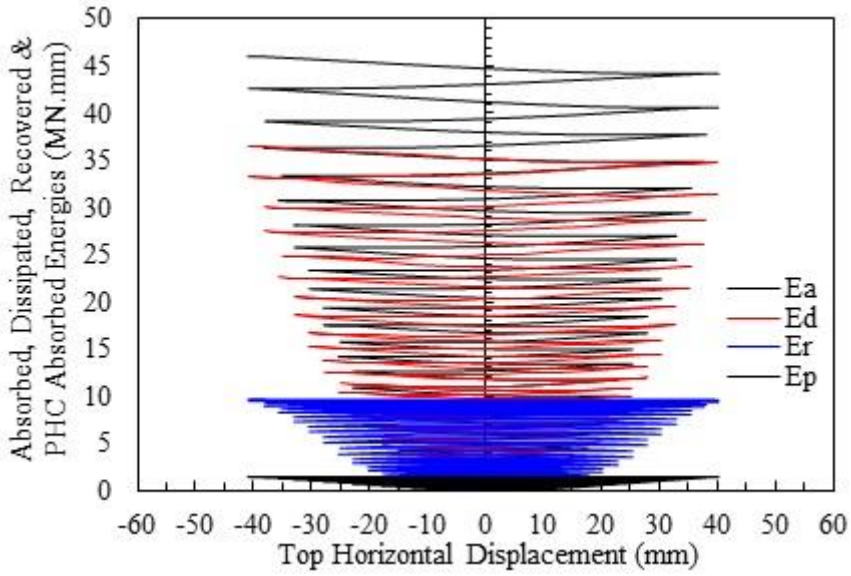

Fig. 3 Different energies versus top amplitude for column C0C3 under cyclic loading

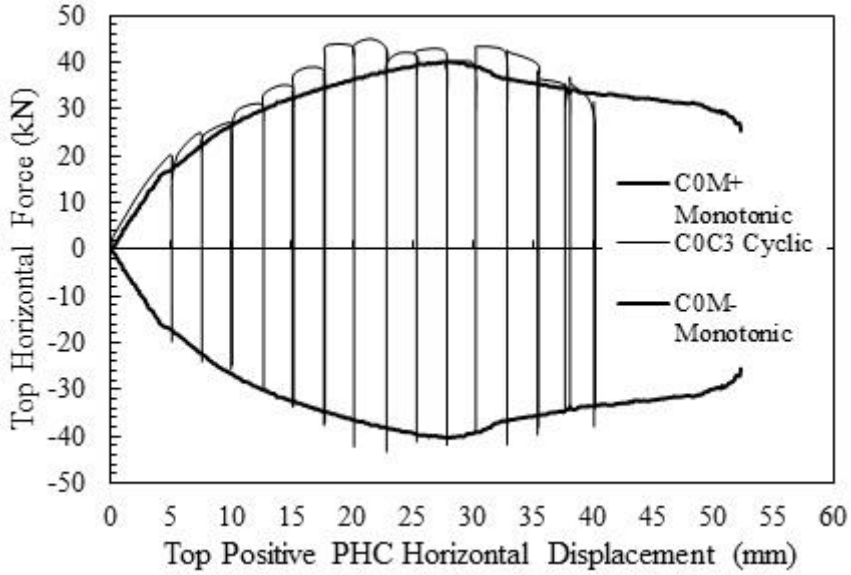

Fig. 4 Force vs. positive PHC displacement, cyclic and monotonic loading

or with a big reduction factor.

In Fig. 4, the variations of the top horizontal force versus only top positive PHC horizontal displacements for cyclic loading of column C0C3 is illustrated and is compared with those of the column C0M under monotonic loading in positive and negative directions. As demonstrated in this figure, in the case of cyclic loading, the force-displacement envelope curve is usually close enough to the monotonic curve, while its maximum displacement at failure is smaller than the maximum displacement obtained monotonically but its maximum force is greater than the maximum force in

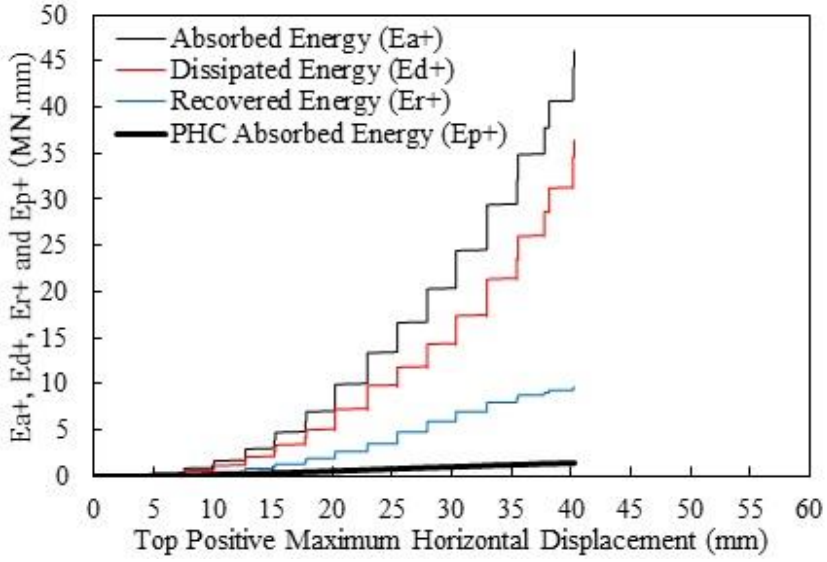

Fig. 5 Different energies versus top amplitudes of column C0C3 under cyclic loading.

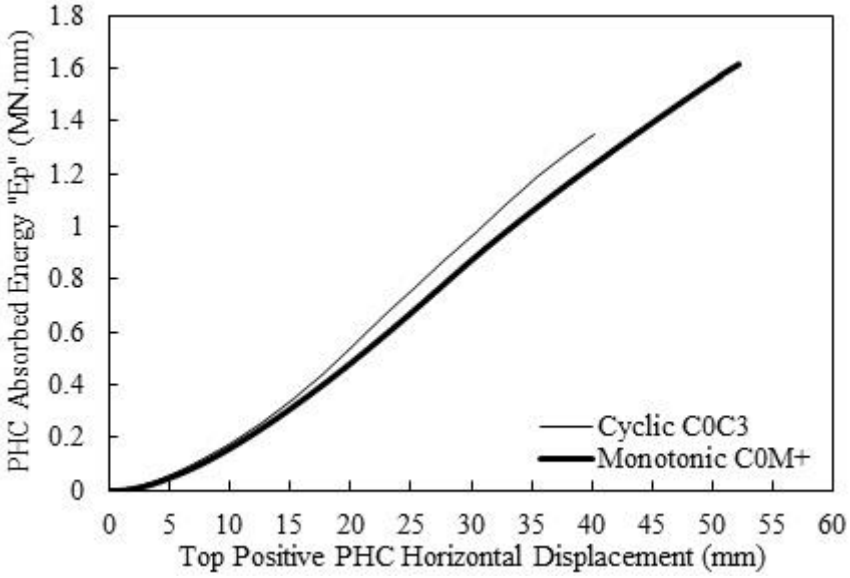

Fig. 6 PHC absorbed energy, calculated for cyclic and monotonic loading

monotonic case. Therefore the small difference between total PHC absorbed energy to failure ($\sum_{i=1}^{i=i} E_{pi}^{+}$) in the cyclic and monotonic loading cases always stand. This can be explained basically by the different types of loading employed.

In Fig. 5 the absorbed, dissipated, recovered and PHC absorbed energies are illustrated versus top PHC positive horizontal displacements for column C0C3 under the cyclic loading.

In Fig. 6 the PHC absorbed energies for columns C0C3 and C0M under the cyclic and monotonic loading are illustrated versus top PHC positive horizontal displacements. A quasi-linear

relationship connecting the PHC absorbed energy to the PHC positive displacements for cyclic and monotonic loading can be observed as shown in Fig. 6.

Within the range of energies studied, the PHC absorbed energy, calculated for cyclic and monotonic loading cases, are very similar.

Since the experimental test results indicate that the damage to the structural members is caused mainly due to the primary half-cycles, the PHC absorbed energy is emphasized and used as the key element in the DI proposed by the authors and the secondary energy explain the fatigue phenomenon of the structural member. The similarity between the absorbed energy of PHC calculated for cyclic and monotonic loading cases is the basis of the DI implicit and explicit versions (given in sections 4.6.1 and 4.6.2) which treat the absorbed energy of PHC of monotonic loading as the normalizing factor and use C^+ and C^- as adaptation factors for covering the differences between cyclic and monotonic cases (see Eqs. (1)-(11)).

Since in these existing damage indices, absorbed energy to failure of monotonic loading is used as a normalizing factor for cyclic loading cases, some adaptation measures are required. Meyer and Garstka have fixed the extreme limits of DI (zero and 100% at intact and failure states), but their distribution between zero and 100% especially for repeated cycles is not valid (confirmed by Garstka 1993).

4.4 Characteristics of an efficient damage index

The real damage caused to structural members should be evaluated by using an efficient quantitative ratio of damage (damage index) applicable for the different types of structural members and the different kinds of loading with different loading history.

The DI must be a representative of damage by showing:

- the realistic visual shape of each damaging phase,
- realistic strength degree and stability of structural member for each damaging phase,
- numerical values increasing from 0% up to 100% for intact status to failure.

4.5 Schematic examples of applying PHC and FHC absorbed energies in DI

The evaluation of the PHC and FHC absorbed energies and DI is illustrated by the following examples shown schematically in Figs. 7 and 8 for cyclic and monotonic loading.

Fig. 7 shows typical top horizontal force-displacement curve of a reinforced concrete column under cyclic loading. The energy E_{p1}^+ of first PHC corresponds to the under curve area of *OAA*', whereas E_{f1}^+ is still zero. If point *A* corresponded to failure, E_{p1}^+ would be equal to $\sum_{i=1}^{i=i} E_{pimax}^+$ and E_u^+ while $i=i_{max}=n=1$ and DI=100%. This concept retains its validity for monotonic loading at failure, similar to the case shown in Fig. 8.

During unloading toward point *B*, the recovered energy corresponding to the area under the curve *AA'B*, is recovered, while the DI retains its value. Following the loading cycle to the point *C*, is a "following half-cycle", with absorbed energy E_{f1}^+, corresponding to the under curve area of BCO. DI^- is still zero. The change in sign of E_{p1}^+, $E_{f1}+$ and E_u^+ occur at the points of symmetry about the origin of the coordinate system. For the first PHC in the negative displacement range, E_{p1}^- is equal to the area under the curve OCDD'. The recovered energy between points *D* and *E* is not considered, and DI retains its value. For loading between points *E* and *F* (first FHC in the negative direction), E_{f1}^- is equal to the area under the curve EFO. Further loading in the positive direction up to point *A*" (maximum positive displacement to date) is equal to a new FHC. The area

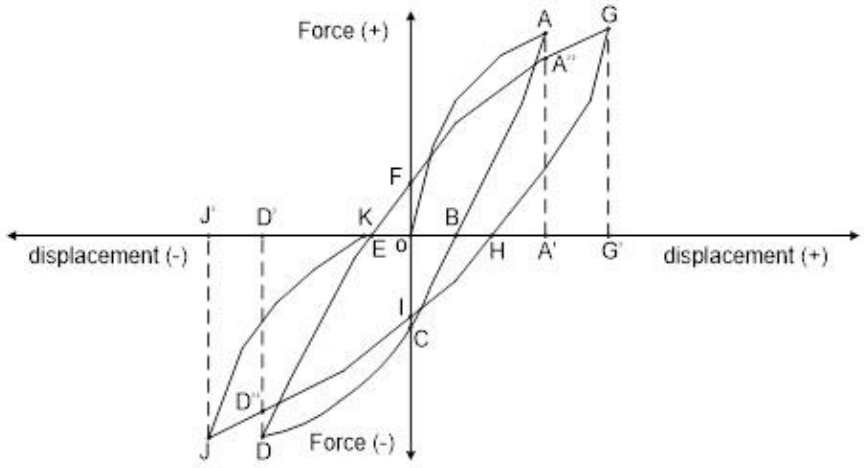

Fig. 7 Schematic illustration of DI calculation procedure for cyclic loading

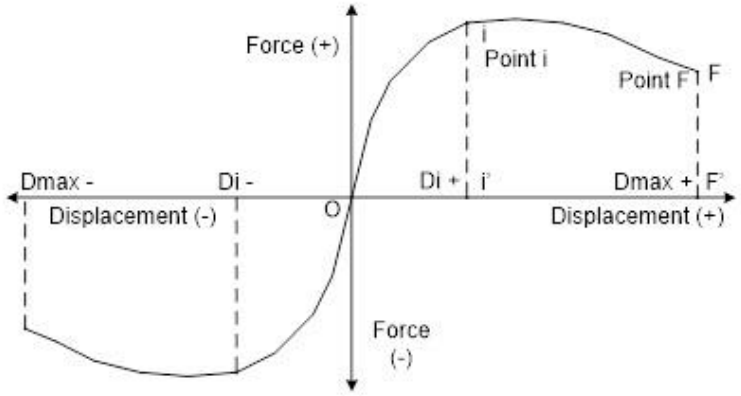

Fig. 8 Schematic illustration of DI calculation procedure for monotonic loading

under the curve *OFA''A*' is equal to E_{f2}^{+}. After point *A*", a new PHC for positive displacements is formed. E_{p2}^{+} is equal to the area under the curve *A''GG'A'*. Subsequent cycles are analyzed with the same procedure and DI is calculated.

Fig. 8 shows the schematic horizontal force-displacement curve of a reinforced concrete column under monotonic loading. Actually monotonic loading is a particular case of cyclic loading with the number of loading cycles being equal to one (either in the positive or negative directions). The total positive PHC absorbed energy $\sum_{i=1}^{i=i} E_{pi}^{+}$ at point i corresponds to the area under the curve (area of *Oii*'). If point *i* corresponded to failure, $\sum_{i=1}^{i=i} E_{pi}^{+}$ would be equal to $\sum_{i=1}^{i=n} E_{pi}^{+}$ and E_{u}^{+} while i=n=1 and DI=100%.

4.6 Proposed global damage index

4.6.1 Damage index (implicit global version)

In the case of cyclic loading, the force-displacement envelope curve is usually close enough to

the monotonic curve (see Fig. 4), while its maximum displacement at failure is smaller than the maximum displacement obtained monotonically but its maximum force is greater than the maximum force in monotonic case. Therefore, the difference between $\sum_{i=1}^{i=i} E_{pi}^{+}$ and E_u^{+} and also between $\sum_{i=1}^{i=i} E_{pi}^{-}$ and E_u^{-} always stand at failures. This can be explained basically by the different methods of loading employed.

The proposed DI expression is equal to the maximum value of DI^+ and DI^-, considering DI^+ for the positive displacements and DI^- for the negative displacements as follows

$$DI = Max[DI^{+},\ DI^{-}] \tag{1}$$

With

$$DI^{+} = \frac{\sum_{i=1}^{i=i} E_{pi}^{+}}{E_u^{+}} \times C^{+} \qquad \text{(for displacements in positive direction)} \tag{2}$$

$$DI^{-} = \frac{\sum_{i=1}^{i=i} E_{pi}^{-}}{E_u^{-}} \times C^{-} \qquad \text{(for displacements in negative direction)} \tag{3}$$

Where:

The adaptation factors "C^+ and C^+" are expressed as follows

$$C^{+} = \frac{(F_{max}^{+} \times \delta_{max}^{+})_{Monotonic}}{(F_{max}^{+} \times \delta_{max}^{+})_{Cyclic}} \tag{4}$$

$$C^{-} = \frac{(F_{max}^{-} \times \delta_{max}^{-})_{Monotonic}}{(F_{max}^{-} \times \delta_{max}^{-})_{Cyclic}} \tag{5}$$

and:

i: cycle number

E_{pi}^{+}: absorbed energy during $(PHC)_i^+$ in positive direction,

E_{pi}^{-}: absorbed energy during $(PHC)_i^-$ in negative direction,

F_{max}^{+} : maximum force applied in positive direction,

F_{max}^{-} : maximum force applied in negative direction,

δ_{max}^{+} : maximum displacement in positive direction,

δ_{max}^{-}: maximum displacement in negative direction,

E_u^{+}: absorbed energy at failure in the case of positive monotonic loading,

E_u^{-}: absorbed energy at failure in the case of negative monotonic loading.

In the DI formulae, E_u^+ and E_u^- are used to represent a normalizing factor while the C^+ and C^- represent adaptation factors, and provide a good relationship between monotonic and cyclic cases when DI is calculated. The effects of the following half-cycles are implicitly taken into account in the C^+ and C^- factors.

This implicit version represents both limits for DI (from 0% up to approximately 100% at failure) and also a realistic progression of the DI factor between these limits. One of the advantages of this version of DI is that, it allows the comparison of the results with those of the monotonic loading case

The developed form of Eqs. (2) and (3) combined with the Eqs. (4) and (5) are written as follows:

$$DI^{+} = \frac{\sum_{i=1}^{i=i} \int_{\delta_{p(i-1)}^{+}}^{\delta_{pi}^{+}} F_{pi}^{+}.d\delta_{pi}^{+}}{E_u^{+}} \times \frac{(F_{max}^{+} \times \delta_{max}^{+})_{monotonic}}{(F_{max}^{+} \times \delta_{max}^{+})_{cyclic}} \quad \text{(for displacements in positive direction)} \tag{6}$$

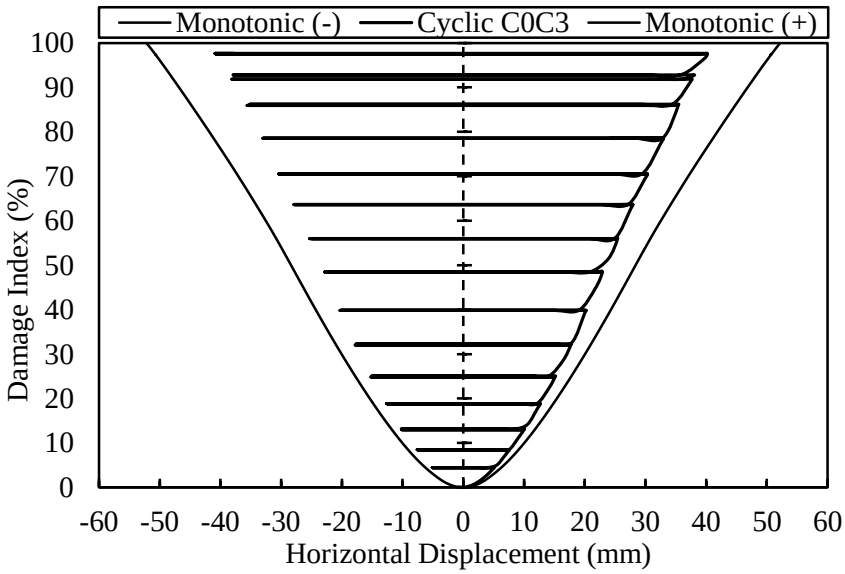

Fig. 9 DI (implicit version) for cyclic (COC3) and monotonic (COM) loading

$$DI^{-} = \frac{\sum_{i=1}^{i=i} \int_{\delta^{-}_{p(i-1)}}^{\delta^{-}_{pi}} F^{-}_{pi}.d\delta^{-}_{pi}}{E^{-}_{u}} \times \frac{(F^{-}_{max} \times \delta^{-}_{max})_{monotonic}}{(F^{-}_{max} \times \delta^{-}_{max})_{cyclic}} \quad \text{(for displacements in negative direction)} \quad (7)$$

Where:

F^{+}_{pi} : applied force during $(PHC)_i^{+}$ in positive direction,

F^{-}_{pi} : applied force during $(PHC)_i^{-}$ in negative direction,

δ^{+}_{pi}: displacement during $(PHC)_i^{+}$ in positive direction,

δ^{-}_{pi} : displacement during $(PHC)_i^{-}$ in negative direction.

Therefore, to apply the global implicit energy-based DI, Eqs. (1), (6) and (7) are used.

In Fig. 9, the proposed implicit DI calculated for cyclic (COC3) and monotonic (COM) loading versus top horizontal displacement in the positive direction is illustrated.

As is demonstrated in Fig. 9, in the proposed implicit vision of DI, since a monotonic normalizing factor and an adaptation factor are used which both depend upon the behaviors of two different columns, the value of DI is not exactly 100% at failure phase (e.g., DI at failure phase, reaches 99% for column C0C1, 102.7% for column C0C2 and 97.7% for column C0C3).

4.6.2 Damage index (explicit global version) for fatigue case

Considering directly the weighting of FHC, the formulas (2) and (3) can be reformulated as (8) and (9), respectively. This explicit version which consists of Eqs. (1), (8) and (9), yields Eqs. (13), (14) and (15) for estimating the number of cycles at failure due to fatigue as follows.

$$DI^{+} = \frac{\sum_{i=1}^{i=i} E^{+}_{pi} + \sum_{j=1}^{j} \sum_{k=1}^{k} \lambda^{+}_{j} E^{j+}_{fk}}{E^{+}_{u}} \quad \text{(for displacements in positive direction)} \quad (8)$$

$$DI^{+} = \frac{\sum_{i=1}^{i=i} E_{pi}^{-} + \sum_{j=1}^{j} \sum_{k=1}^{k} \lambda_j^{-} E_{fk}^{j-}}{E_u^{-}} \qquad \text{(for displacements in negative direction)} \qquad (9)$$

Where:

i: cycle number (considering all cycles, equals $j \times k$ for regular repeating cases),

j: group number of constant amplitude cycles,

k: number of cycles in group j,

E_{fk}^{j+}: absorbed energy during $(FHC)_k^{+}$ at each different amplitude number j,

λ_j^{+}: fatigue factor for group j (for positive displacements),

E_{fk}^{j-}: absorbed energy during $(FHC)_k^{-}$ at each different amplitude number j,

λ_j^{-}: fatigue factor for group j (for negative displacements).

The developed form of Eqs. (8) and (9) are written as follows:

$$DI^{+} = \frac{\sum_{i=1}^{i=i} \int_{\delta_{p(i-1)}^{+}}^{\delta_{pi}^{+}} F_{pi}^{+}.d\delta_{pi}^{+} + \sum_{j=1}^{j} \sum_{k=1}^{k} \int_{\delta_{f(k-1)}^{j+}}^{\delta_{fk}^{j+}} \lambda_j^{+} F_{fk}^{j+}.d\delta_{fk}^{j+}}{E_u^{+}} \qquad \text{(for positive displacements)} \qquad (10)$$

$$DI^{-} = \frac{\sum_{i=1}^{i=i} \int_{\delta_{p(i-1)}^{-}}^{\delta_{pi}^{-}} F_{pi}^{-}.d\delta_{pi}^{-} + \sum_{j=1}^{j} \sum_{k=1}^{k} \int_{\delta_{f(k-1)}^{j-}}^{\delta_{fk}^{j-}} \lambda_j^{-} F_{fk}^{j-}.d\delta_{fk}^{j-}}{E_u^{-}} \qquad \text{(for negative displacements)} \qquad (11)$$

Where:

δ_{fk}^{j+}: displacement during $(FHC)_k^{+}$ at each different amplitude number j,

δ_{fk}^{j-}: displacement during $(FHC)_k^{-}$ at each different amplitude number j.

The following half-cycles cannot be taken into account without weighting them. This has also been noticed during the tests of Sieffert *et al*. (1990). Therefore the reducing factors λ_j^{+} and λ_j^{-} (essentially depending on the number of cycles) for the fixed amplitude a_j^{+} and a_j^{-} should be included. These factors are calculated locally for successive $\delta_{\max}^{+}$ and $\delta_{\max}^{-}$, by equating the Eqs. (6) and (10) and the Eqs. (7) and (11) respectively.

Therefore, to apply the global explicit energy-based DI, Eqs. (1), (10) and (11) are used.

4.6.3 Estimation of the number of cycles at failure due to fatigue

An additional advantage of this form of explicit DI is that makes it possible to estimate the number of cycles at failure (n_j) due to fatigue.

At failure DI=1, assuming that the loop areas remain constant up to failure, this means that the absorbed energy is still the same during each following cycle (i.e.: E_{fk}^{j+} is constant and equals to E_{f1}^{j+} for identical cycles of set type j. Similarly for negative displacements E_{fk}^{j-} is constant and equals to E_{f1}^{j-} for identical cycles set type j). In this case $\sum_{i=1}^{i=i} E_{pi}^{+} = E_{p1}^{+}$ and $\sum_{i=1}^{i=i} E_{pi}^{-} = E_{p1}^{-}$. The difference between E_u^{+} and $\sum_{i=1}^{i=i} E_{pi}^{+}$ in monotonic and cyclic loading cases at failure (the area under the curve CMM'C' shown in Fig. 10) is due to the effect of the following half-cycle absorbed energy ($\sum_{j=1}^{j} \sum_{k=1}^{k} \lambda_j^{+} E_{fk}^{j+}$) which for identical cycles set type j equates to $n_j \lambda_j^{+} E_{f1}^{j+}$ and ($\sum_{j=1}^{j} \sum_{k=1}^{k} \lambda_j^{-} E_{fk}^{j-}$) equates to $n_j \lambda_j^{-} E_{f1}^{j-}$.

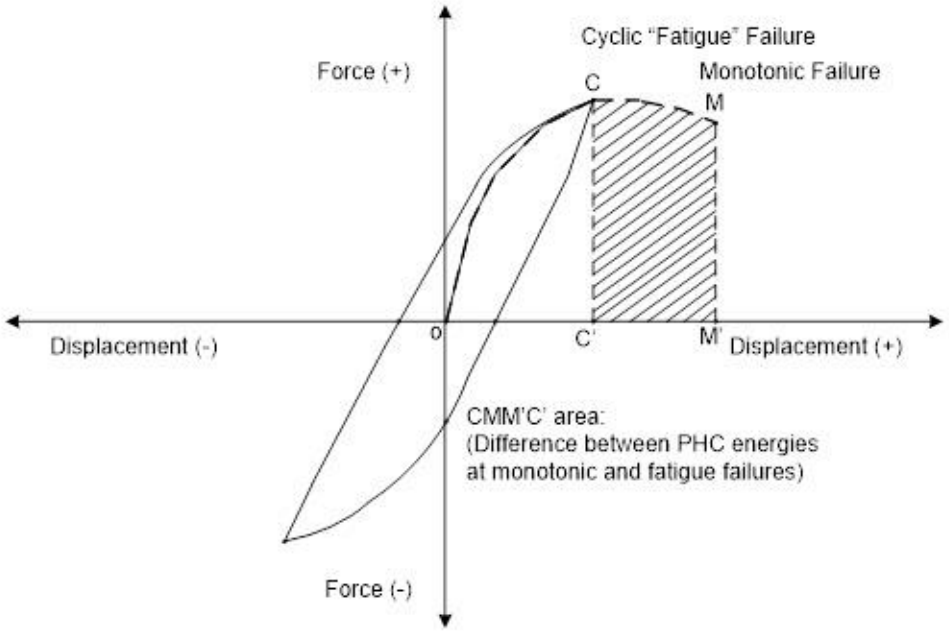

Fig. 10 The difference between E_u^+ and $\sum_{i=1}^{i=i} E_{pi}^+$ in monotonic and cyclic cases at failure

According to this discussion n_j is obtained as follows for these identical cycles set type j

$$DI = Max[DI^+,\ DI^-] = 1 \tag{12}$$

$$n_j = Min\ [n_j^+, n_j^-] \tag{13}$$

With:

$$n_j^+ = \frac{E_u^+ - E_{p1}^+}{\lambda_j^+ E_{f1}^{j+}} \qquad \text{(If at failure: DI = DI}^+\text{, or for DI}^+ > \text{DI}^-\text{)} \tag{14}$$

$$n_j^- = \frac{E_u^- - E_{p1}^-}{\lambda_j^- E_{f1}^{j-}} \qquad \text{(If at failure: DI = DI}^-\text{, or for DI}^+ < \text{DI}^-\text{)} \tag{15}$$

Where:

E_{p1}^+: absorbed energy for a $(PHC)_j^+$,

E_{f1}^{j+}: absorbed energy for an $(FHC)_j^+$,

E_{p1}^-: absorbed energy for a $(PHC)_j^-$,

E_{f1}^{j-}: absorbed energy for an $(FHC)_j^-$.

The test results show that λ_j^+ and λ_j^- are variable versus amplitude.

The developed form of Eqs. (13) and (14) are written as follows:

$$n_j^+ = \frac{E_u^+ - \int_0^{\delta_{p1}^+} F_p^+ . d\delta_p^+}{\lambda_j^+ \int_0^{\delta_{f1}^{j+}} F_f^{j+} . d\delta_f^{j+}} \qquad \text{(If at failure: DI = DI}^+\text{, or for DI}^+ > \text{DI}^-\text{)} \tag{16}$$

$$n_j^- = \frac{E_u^- - \int_0^{\delta_{p1}^-} F_p^- . d\delta_p^-}{\lambda_j^- \int_0^{\delta_{f1}^{j-}} F_f^{j-} . d\delta_f^{j-}} \qquad \text{(If at failure: DI = DI}^-\text{, or for DI}^+ < \text{DI}^-\text{)} \qquad (17)$$

Where:

δ_{p1}^+: maximum displacement for a $(PHC)_j^+$,

δ_{f1}^{j+}: maximum displacement for an $(FHC)_j^+$,

δ_{p1}^-: maximum displacement for a $(PHC)_j^-$,

δ_{f1}^{j-}: maximum displacement for an $(FHC)_j^-$.

Therefore, to find the number of cycles at failure due to fatigue Eq. (13), (16) and (17) are used.

Fig. 11 shows the λ_j^+ for cycles producing failure versus a_j^+ amplitudes at failure for cyclic loading based on the used experimental test data (Garcia Gonzalez 1990, and Sieffert *et al*. 1990). In this case the following equation is found for λ_j^+

$$\lambda_j^+ = 0.1719 \times (a_j^+)^{(-1.462)} \qquad (a_j^+ \text{ in mm}) \qquad (18)$$

Fig. 12 shows the estimated number of cycles producing failure (n_j) versus different chosen amplitudes at failure for cyclic loading. In the particular case of a monotonic loading (i.e., n=1) from best-fit curve shown in Fig. 12, maximum displacement at failure is obtained at approximately 57.5 mm while it was found to be 53 mm in the real monotonic experimental test. This corresponds to an 8.5% relative difference.

For the tested columns the following equation is found for n_j

$$n_j = -793.4 \times lna_j + 3214 \qquad (a_j \text{ in mm}) \qquad (19)$$

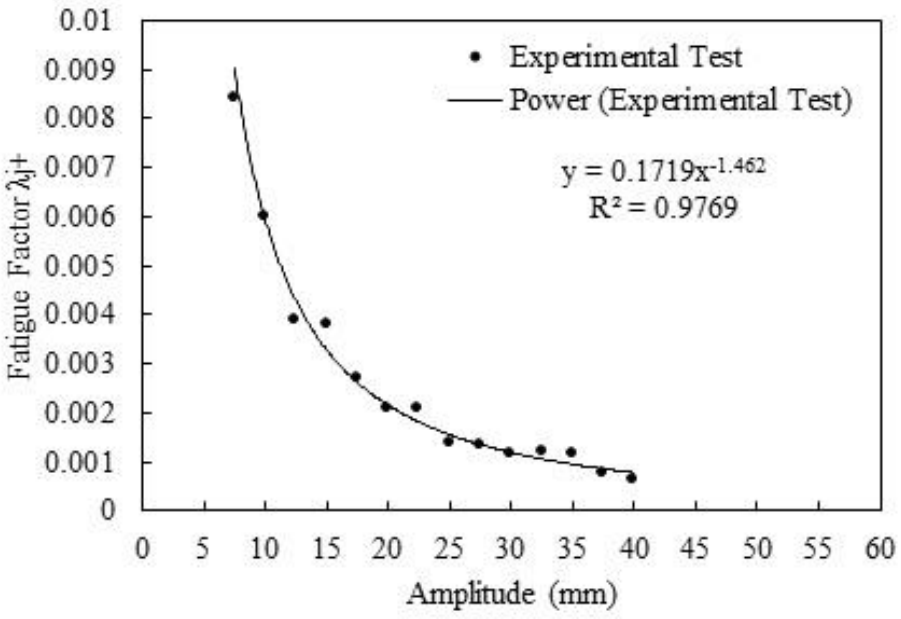

Fig. 11 λ_j^+ for cycles producing failure

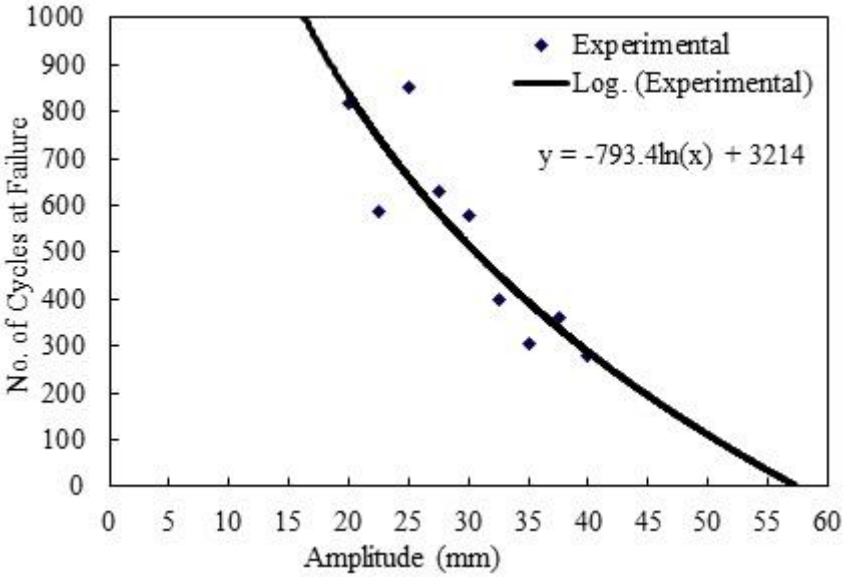

Fig. 12 n_j versus different chosen amplitudes at failure for cyclic loading

4.6.4 Damage index (simplified global version)

This version is simple, direct and more exact at failure for the cases of cyclic loading, but it is not valid for fatigue loading.

In this version the summation of PHC absorbed energy to any cycle is normalized to the summation of PHC absorbed energy to failure for the same cyclic loading and on the same structural member. Since in this version, the same cyclic loading model and structural member are used for damage values and normalizing factor, DI reaches exactly 100% at failure. In this case, a monotonic loading test is not needed for the cyclic loading case (Sadeghi 2011).

This simplified version consists of the Eqs. (1), (20) and (21) as follows

$$DI^{+} = \frac{\sum_{i=1}^{i=i} E_{pi}^{+}}{\sum_{i=1}^{i=n} E_{pi}^{+}} \qquad \text{(for displacements in positive direction)} \qquad (20)$$

$$DI^{-} = \frac{\sum_{i=1}^{i=i} E_{pi}^{-}}{\sum_{i=1}^{i=n} E_{pi}^{-}} \qquad \text{(for displacements in negative direction)} \qquad (21)$$

The developed form of Eqs. (20) and (21) are written as follows

$$DI^{+} = \frac{\sum_{i=1}^{i=i} \int_{\delta_{p(i-1)}}^{\delta_{pi}} F_{pi}^{+}.d\delta_{pi}^{+}}{\sum_{i=1}^{i=n} \int_{\delta_{p(i-1)}}^{\delta_{pi}} F_{pi}^{+}.d\delta_{pi}^{+}} \qquad \text{(for displacements in positive direction)} \qquad (22)$$

$$DI^{-} = \frac{\sum_{i=1}^{i=i} \int_{\delta_{p(i-1)}}^{\delta_{pi}} F_{pi}^{-}.d\delta_{pi}^{-}}{\sum_{i=1}^{i=n} \int_{\delta_{p(i-1)}}^{\delta_{pi}} F_{pi}^{-}.d\delta_{pi}^{-}} \qquad \text{(for displacements in negative direction)} \qquad (23)$$

Therefore, to apply the global simplified DI, Eqs. (1), (22) and (23) are used.

In the implicit and explicit versions, the absorbed energy at the failure of monotonic case

loading is used as a normalizing factor therefore in those cases, DI is approximately 100% at failure and the monotonic test or numerical simulation is applicable. While in the simplified version, DI reaches exactly 100% at failure for cyclic loading and monotonic loading test or numerical simulation is not required.

In Figs. 13 and 14, the simplified DI calculated for cyclic and monotonic loading versus top horizontal displacement in the positive direction is shown.

In Fig. 13, the proposed simplified DI calculated for columns C0C1 and C0M under cyclic and

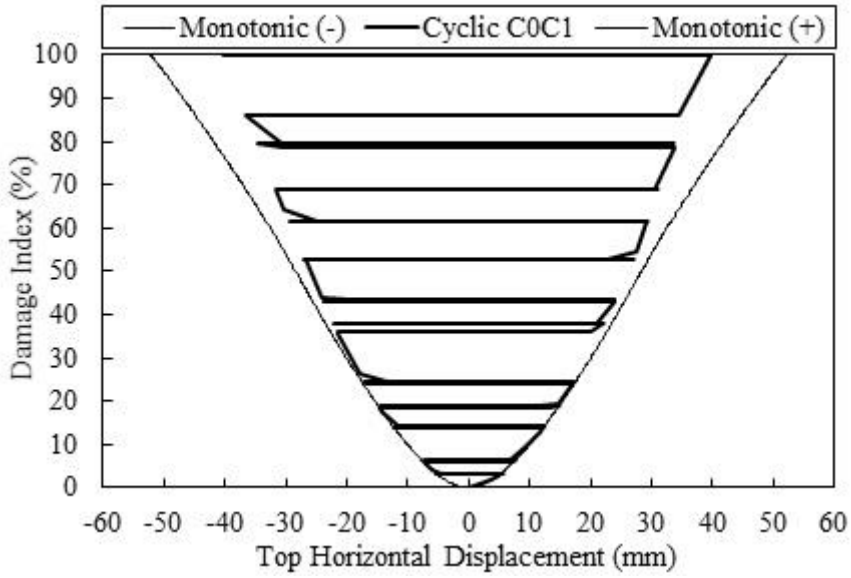

Fig. 13 Proposed simplified DI, calculated for cyclic and monotonic loading, columns C0C1 and C0M

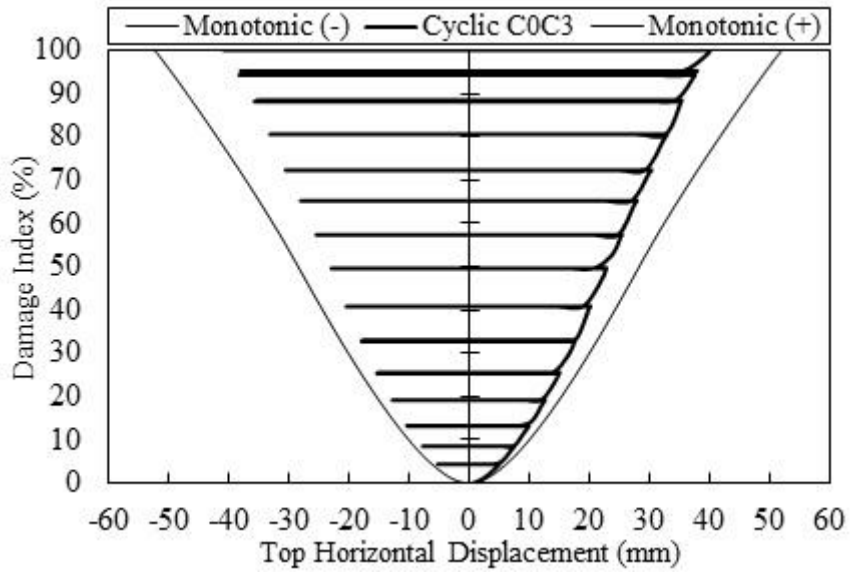

Fig. 14 Proposed simplified DI, calculated for cyclic and monotonic loading, columns C0C3 and C0M

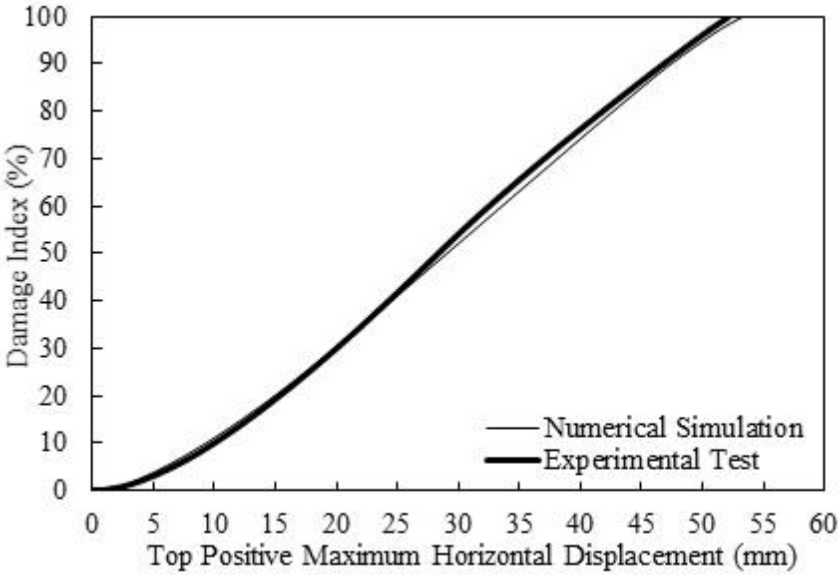

Fig. 15 DI calculated based on experimental and numerical simulation results, monotonic loading case

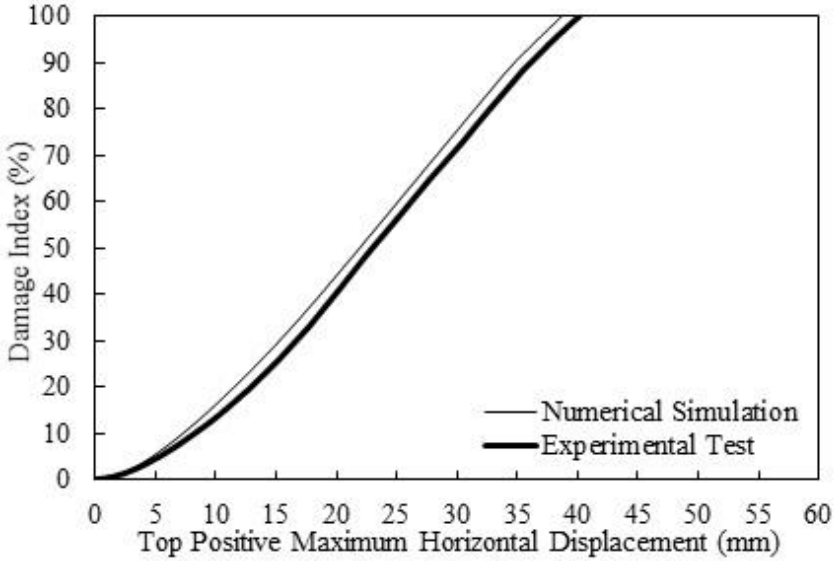

Fig. 16 DI calculated based on experimental and numerical simulation results, cyclic loading case

monotonic loading versus top horizontal displacement are shown. As this figure indicates, in the experimental test, column C0C1 is damaged during both positive and negative displacements, therefore the increasing of DI is due to both "D^{+}" and "D^{-}", while the column C0C3 has been damaged only during positive displacements, as shown in Fig. 14.

Figs. 15 and 16 represent the comparison between values of the proposed simplified global DI calculated based on experimental tests (Garcia Gonzalez 1990, Sieffert *et al*. 1990), and numerical simulation results simulated by using CADEP for monotonic and cyclic loading (C0M and C0C3),

respectively. This comparison shows that for the calculation of DI, performing the expensive experimental tests is not necessary and using an analytical method such as finite element method is sufficient.

4.7 Proposed local damage index

Based on the evidence that the structural member is highly affected in the critical zone (section), the main bending effect is due to the curvature registered at critical sections. Actually, after the peak value on the response curve of the critical section, very significant local effects occur at the critical section where a pseudoplastic hinge appears. Once the peak has passed, curvature enhancement is concentrated in the critical zone (section), while in the other regions, the curvatures decrease rapidly to near zero and cracks openings are closed. To determine force-displacement relationships for different sections of a structural member to apply the global energy-based DI requires a time-consuming calculation of the structural member's displacement. Further, the structural member response is highly affected in the critical zone (section), a comparable local moment-curvature based DI, derived from the global DI is proposed as follows. The calculation of the different terms of the different versions of the proposed local DI is performed using the same procedure as explained in section 4.6 for global DI by replacing force-displacement curve by the moment-curvature curve. The different versions of the proposed local DI are given below.

In general, since there is a strong interaction between local and global behaviors of the columns under lateral loading due to the role of the critical section, the local and global damage indices give approximately similar results, while each of them has its own advantages.

4.7.1 Damage index (implicit local version)

Eqs. (1), (24) and (25) are proposed to calculate the implicit local DI

$$DI^{+} = \frac{\sum_{i=1}^{i=i} \int_{\varphi^{+}_{p(i-1)}}^{\varphi^{+}_{pi}} M^{+}_{pi}.d\varphi^{+}_{pi}}{E^{+}_{mu}} \times \frac{\left(M^{+}_{max} \times \varphi^{+}_{max}\right)_{monotonic}}{(M^{+}_{max} \times \varphi^{+}_{max})_{cyclic}} \quad \text{(for positive loading directions)} \quad (24)$$

$$DI^{-} = \frac{\sum_{i=1}^{i=i} \int_{\varphi^{-}_{p(i-1)}}^{\varphi^{-}_{pi}} M^{-}_{pi}.d\varphi^{-}_{pi}}{E^{-}_{mu}} \times \frac{(M^{-}_{max} \times \varphi^{-}_{max})_{monotonic}}{(M^{-}_{max} \times \varphi^{-}_{max})_{cyclic}} \quad \text{(for negative loading directions)} \quad (25)$$

Where:

M^{+}_{pi}: applied bending moments during $(PHC)_i^{+}$ in positive direction,

M^{-}_{pi}: applied bending moments during $(PHC)_i^{-}$ in negative direction,

φ^{+}_{pi}: curvature during $(PHC)_i^{+}$ for positive PHC curvature,

φ^{-}_{pi}: curvature during $(PHC)_i^{-}$ for negative PHC curvature,

M^{+}_{max} : maximum moment applied in positive direction,

M^{-}_{max} : maximum moment applied in negative direction,

φ^{+}_{max} : maximum curvature in positive direction,

φ^{-}_{max}: maximum curvature in negative direction,

E^{+}_{mu}: area under the curve of moment-curvature at failure in the case of positive monotonic loading,

E^{-}_{mu}: area under the curve of moment-curvature at failure in the case of negative monotonic loading.

Therefore, to apply the local implicit energy-based DI, Eqs. (1), (24) and (25) are used.

4.7.2 Damage index (explicit local version)

Eqs. (1), (25) and (26) are proposed to calculate the explicit local DI

$$DI^{+} = \frac{\sum_{i=1}^{i=i}\int_{\varphi_{p(i-1)}}^{\varphi_{pi}} M_{pi}^{+}.d\varphi_{pi}^{+} + \sum_{j=1}^{j}\sum_{k=1}^{k}\int_{\varphi_{f(k-1)}}^{\varphi_{fk}} \lambda_{j}^{+} M_{fk}^{j+}.d\varphi_{fk}^{j+}}{E_{u}^{+}} \quad \text{(for positive loading directions)} \quad (26)$$

$$DI^{-} = \frac{\sum_{i=1}^{i=i}\int_{\varphi_{p(i-1)}}^{\varphi_{pi}} M_{pi}^{-}.d\varphi_{pi}^{-} + \sum_{j=1}^{j}\sum_{k=1}^{k}\int_{\varphi_{f(k-1)}}^{\varphi_{fk}} \lambda_{j}^{-} M_{fk}^{j-}.d\varphi_{fk}^{j-}}{E_{u}^{-}} \quad \text{(for negative loading directions)} \quad (27)$$

Where:

φ_{fk}^{j+}: curvature during $(FHC)_{k}^{+}$ at each different amplitude number j,

φ_{fk}^{j-}: curvature during $(FHC)_{k}^{-}$ at each different amplitude number j.

4.7.3 Estimation of the number of cycles at failure due to fatigue in local level

Eqs. (13), (28) and (29) are used to estimate the number of cycles at failure due to fatigue in local level

$$n_{j}^{+} = \frac{E_{mu}^{+} - \int_{0}^{\varphi_{p1}} M_{p}^{+}.d\varphi_{p}^{+}}{\lambda_{j}^{+}\int_{0}^{\varphi_{f1}} M_{f}^{j+}.d\varphi_{f}^{j+}} \qquad \text{(If at failure: DI = DI}^{+}\text{, or for DI}^{+} > \text{DI}^{-}\text{)} \qquad (28)$$

$$n_{j}^{-} = \frac{E_{mu}^{-} - \int_{0}^{\varphi_{p1}} M_{p}^{-}.d\varphi_{p}^{-}}{\lambda_{j}^{-}\int_{0}^{\varphi_{f1}} M_{f}^{j-}.d\varphi_{f}^{j-}} \qquad \text{(If at failure: DI = DI}^{-}\text{, or for DI}^{+} < \text{DI}^{-}\text{)} \qquad (29)$$

4.7.4 Damage index (simplified local version)

The Eqs. (1), (30) and (31) are used for calculation of the proposed simplified local DI

$$DI^{+} = \frac{\sum_{i=1}^{i=i}\int_{\varphi_{p(i-1)}}^{\varphi_{pi}} M_{pi}^{+}.d\varphi_{pi}^{+}}{\sum_{i=1}^{i=n}\int_{\varphi_{p(i-1)}}^{\varphi_{pi}} M_{pi}^{+}.d\varphi_{pi}^{+}} \qquad \text{(for positive loading directions)} \qquad (30)$$

$$DI^{-} = \frac{\sum_{i=1}^{i=i}\int_{\varphi_{p(i-1)}}^{\varphi_{pi}} M_{pi}^{-}.d\varphi_{pi}^{-}}{\sum_{i=1}^{i=n}\int_{\varphi_{p(i-1)}}^{\varphi_{pi}} M_{pi}^{-}.d\varphi_{pi}^{-}} \qquad \text{(for negative loading directions)} \qquad (31)$$

5. Relation between different phases of damage and damage index

Table 1 allows comparison of the calculated global DI, on the basis of the different submitted versions and the damaging phase ranges for the tested column C0C3 under cyclic loading.

The results of the calculation of the DI applying implicit, explicit or simplified versions give a regular distribution of structural damages up to failure and are very similar.

6. Practical use of damage index

The practical use of the proposed DI is illustrated schematically in Fig. 17.

Table 1 Global DI and observed damaging phases for the tested column C0C3 under cyclic loading

Damaging phases (Visual observations)	δ_{max}^{+} (mm)	Implicit & explicit DI (%)	Simplified DI (%)
Phase A (First tension cracks)	2.4	1.21	1.24
	5.0	4.45	4.56
	7.5	8.48	8.68
Phase B (Tension crack development)	10.1	13.15	13.46
	12.6	18.85	19.30
	15.2	25.08	25.69
	17.8	32.31	33.09
	20.2	39.83	40.79
Phase C (First compression cracks appearance)	22.4	48.47	49.63
Phase D (Compression cracks development)	25.4	55.99	57.33
	27.9	63.64	65.17
	30.3	70.53	72.23
	32.9	78.55	80.44
Phase E (Failure of column)	35.5	86.21	88.28
	38.1	92.80	95.04
	40.2	97.65	100.00

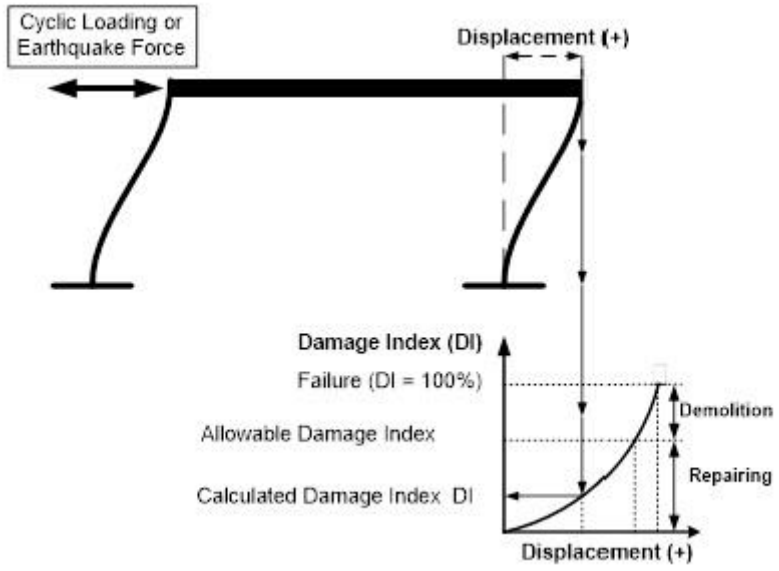

Fig. 17 Schematic illustration of the practical use of DI

In order to calculate the global DI, the force-displacement data and to calculate the local DI, the moment-curvature data for the critical section are required. This data can be found from numerical simulation of structures. In deciding after an earthquake, whether to repair or demolish a structure, the calculated DI is compared with an allowable damage index ($\overline{DI}$) which could be determined by technical rules and practice codes for different types of structures according to cost and safety

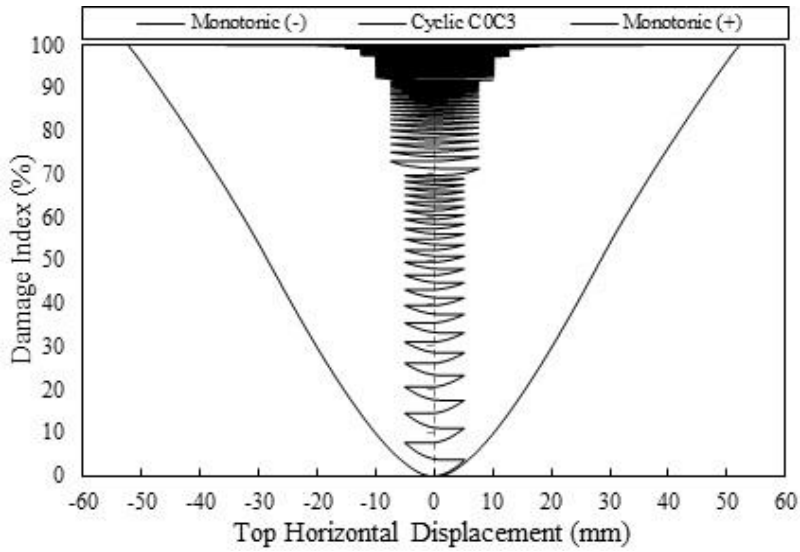

Fig. 18 Meyer's DI, calculated for tested columns under cyclic and monotonic loading

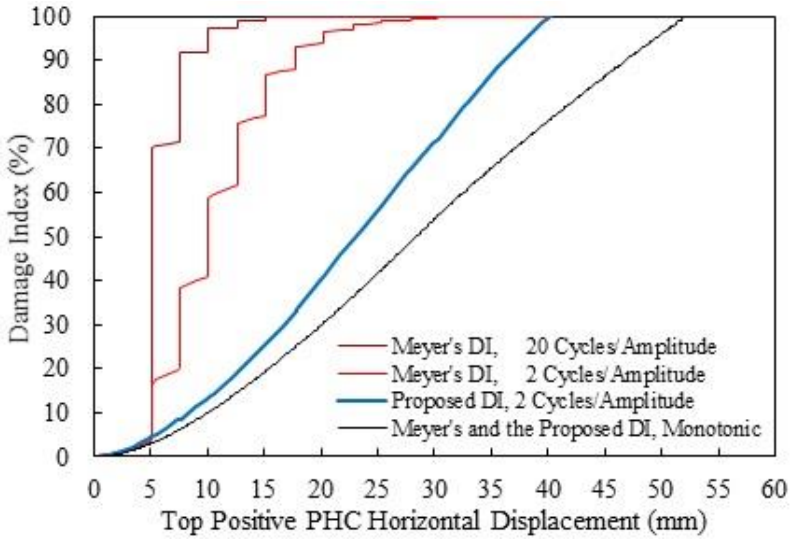

Fig. 19 Comparison of the proposed and Meyer's damage indices calculated for different loading cases

criteria (see Fig. 17).

For the tested RC columns under cyclic oriented lateral loading and axial loading, the values of the proposed DI, reached about 5% in the phase of the first tensile cracks appearance, about 45% when the first compression cracks occurred, and 100% at failure.

7. Comparison of the proposed and Meyer's damage indices

In Fig. 18, the Meyer's index calculated for columns C0C3 and C0M under cyclic and

monotonic loading, versus top horizontal displacement are presented. Comparison of the values given in Figs. 13, 14 and 18 with damage phases show that the DI proposed by Meyer is oversensitive to the number of cycles and is therefore, not applicable in the case of loading comprising repeated cycles, while the proposed DI provides a regular distribution adapted to different phases of damage up to failure for any type of loading.

In monotonic loading cases, the proposed index and Meyer's index provide exactly the same results.

In Fig. 19, the proposed global DI calculated for columns C0C3 and C0M under cyclic and monotonic loading and Meyer's index versus top PHC horizontal displacement in the positive direction are compared. As shown in this figure, the DI proposed by Meyer is oversensitive to the number of cycles and is therefore, not applicable in the case of loading comprising repeated cycles. For example, applying the column test results under cyclic loading with 20 repeated cycles per amplitude shows that Meyer's DI reaches 70% in the phase of first tension crack appearance at the amplitude of 5 mm, and 99.9% in the phase of compression cracks appearance at the amplitude of 22.5 mm, while in these phases the proposed DI reaches 4.5% and about 49%, respectively.

8. Conclusions

The different versions of the DI proposed in this paper are applicable to RC structures subjected to both cyclic and monotonic loading. They have been validated both by comparing the experimental data obtained in laboratory tests and by nonlinear numerical simulation. They are practical, quick and cost-effective means for determining whether to repair or demolish structures after an earthquake or any other type of cyclic loading. They can also be employed in the design of new structures as design parameters. The values of the proposed DI, reached approximately 5% in the phase of the first tensile cracks appearance, about 50% when the first compression cracks occurred, and 100% at failure. The index considers the real temporal sequence of loading cycles, providing a regular distribution adapted to different phases of damage up to failure and can be applied to RC structures under both cyclic and monotonic loading in any direction. The comparison between values of the proposed DI calculated based on experimental test data and numerical simulation results for a cyclic loading case shows that to calculate DI, performing the expensive experimental tests is not necessary and using a nonlinear structural analytical simulation is sufficient. To apply this index, the force-displacement or moment-curvature data of the structural member is required for the global or local approaches, respectively. In general, since there is a strong interaction between local and global behaviors of the columns under lateral loading, due to the role of the critical section, the local and global damage indices give approximately similar results, while each of them has its own advantages.

References

Abbasnia, R., Mirzadeh, N. and Kildashti, K. (2011), "Assessment of axial force effect on improved damage index of confined RC beam-column members", *Int. J. Civil Eng.*, **9** (3), 237-246.

Amaravel, R. and AppaRao, G. (2015), "Studies on various theories and models for assessing the remaining life of damaged railway bridges-review (fatigue and fracture mechanics approach)", *Int. Res. J. Eng. Tech.*, **2**(5), 183-195.

Amziane, S. and Dubé, J.F. (2008), "Global RC structural damage index based on the assessment of local material damage", *J. Adv. Concrete Tech.*, **6**(3), 459-468.
Cao, V.V., Ronagh, H.R., Ashraf, M. and Baji, H. (2014), "A new damage index for reinforced concrete structures", *Earthq. Struct.*, **6**(6), 581-609.
CEB Code (1978), "Code-Modéle CEB-FIP pour les structures en béton", Bulletin d'information no. 124-125F, *Comité Euro-International du Béton*, Vol. 1-2, Paris.
Changfeng, T., Liang, W. and Qiang, Z. (2012), "Fatigue reliability analysis on the concrete beams", *Proceedings of 2012 International Conference on Mechanical Engineering and Material Science (MEMS 2012)*, Yangzhou, China.
Garcia Gonzalez, J.J. (1990), "Contribution á l'étude des poteaux en béton armé soumis á un cisaillement dévié alterné", Ph.D. Dissertation, University of Nantes/Ecole Central de Nantes, Nantes.
Garstka, B. and Stangenberg, F. (1993), "Damage assessment in cyclically loaded reinforced concrete members", *Proceedings of The Second European Conference on Structural Dynamics*, Structural Dynamics, Vol. 1, Trondheim, Norway.
Iranmanesh, A. and Ansari, F. (2014), "Energy-based damage assessment methodology for structural health monitoring of modern reinforced concrete bridge columns" *J. Bridge Eng.*, ASCE, **19**(8), A4014004.
Li, K., Wang, X. L., Cao, S. Y. and Chen, Q. P. (2015), "Fatigue behavior of concrete beams reinforced with HRBF500 steel bars", *Struct. Eng. Mech.*, **53**(2), 311-324.
Massumi, A. and Monavari, B. (2013), "Energy based procedure to obtain target displacement of reinforced concrete structures", *Struct. Eng. Mech.*, **48**(5), 681-695.
Meyer, I.F., Kratzig, W.B., Stangenberg, F. and Maeskouris, K. (1988), "Damage prediction in reinforced concrete frames under seismic actions", *Eur. Earthq. Eng.*, **3**, 9-15.
Olsson, K. and Peterson, J. (2010), "Fatigue assessment methods for reinforced concrete bridges in Euro code", Chalmers University of Technology, Goteborg, Sweden.
Otes, A. (1985), "Zur werkstoffgerechten Berechnung der Erdbebenbeanspruchng in Stahlbetontragwerken", Mitteilungen aus dem Institut für Massivbau der TH Darmstadt, Heft 25, Bochum, Germany.
Paal, S., Jeon, J., Brilakis, I. and DesRoches, R. (2014). "Automated damage index estimation of reinforced concrete columns for post-earthquake evaluations", *J. Struct. Eng.*, ASCE, **141**(9), 04014228..
Park, Y.J. and Ang, A.H.S. (1985), "Mechanistic seismic damage model for reinforced concrete", *J. Struct. Div.*, ASCE, **111**(4), 722-739.
Park, R., Kent, D.C. and Sampson, R.A. (1972), "Reinforced concrete members with cyclic loading", *J. Struct. Div.*, ASCE, **98**(ST7), 1341-1359.
Priestley, M.J.N. and Park, R. (1987), "Strength and durability of concrete bridge columns under seismic loading", *ACI Struct. J.*, **84**(1), 61-76.
Rodrigueza, M.E. and Padillaa, D. (2009), "A damage index for the seismic analysis of reinforced concrete members", *J. Earthq. Eng.*, **13**(3), 364-383.
Sadeghi, K. (2011), "Energy based structural damage index based on nonlinear numerical simulation of structures subjected to oriented lateral cyclic loading", *Int. J. Civil Eng.*, **9**(3), 155-164.
Sadeghi, K. (2014), "Analytical stress-strain model and damage Index for confined and unconfined concretes to simulate RC structures under cyclic loading", *Int. J. Civil Eng.*, **12**(3), 333-343.
Sadeghi, K. (2015), "Nonlinear numerical simulation of RC columns subjected to cyclic oriented lateral force and axial loading", *Struct. Eng. Mech.*, **53**(4), 745-765.
Sieffert, J.G., Lamirault, J. and Garcia, J.J. (1990), "Behavior of R/C columns under static compression and lateral cyclic displacement applied out of symmetrical planes", *Proceedings of the First European Conference on Structural Dynamics (EUROPEAN 90)*, Vol. 1, Bochum, Germany.
Sheikh, S.A. (1982), "A comparative study of confinement models", *ACI J.*, ***79***(4), 296-305.
Zhu, J., Chen, C. and Han, Q. (2014), "Vehicle bridge coupling vibration analysis based fatigue reliability prediction of prestressed concrete highway bridges", *Struct. Eng. Mech.*, **49**(2), 203-223.